Anisotropic physical properties of single-crystal U_2Rh_2Sn in high magnetic fields

K. Prokeš,[1,*] D. I. Gorbunov,[2] M. Reehuis,[1] B. Klemke,[1] A. Gukasov,[3] K. Uhlířová,[4] X. Fabrèges,[3] Y. Skourski,[2] F. Yokaichiya,[1] S. Hartwig,[1] and A. V. Andreev[5]

[1]*Helmholtz-Zentrum Berlin für Materialien und Energie, 14109 Berlin, Germany*

[2]*Dresden High Magnetic Field Laboratory (HLD-EMFL), Helmholtz-Zentrum Dresden-Rossendorf, 01314 Dresden, Germany*

[3]*Laboratoire Léon Brillouin, CEA, CNRS, Université Paris-Saclay, CEA-Saclay, 91191 Gif-sur-Yvette, France*

[4]*Faculty of Mathematics and Physics, Charles University, 121 16 Praha 2, The Czech Republic*

[5]*Institute of Physics, Academy of Sciences of the Czech Republic, 182 21 Prague, Czech Republic*

(Received 26 October 2016; revised manuscript received 14 March 2017; published 22 May 2017)

We report on the crystal and magnetic structures, magnetic, transport, and thermal properties of U_2Rh_2Sn single crystals studied in part in high magnetic fields up to 58 T. The material adopts a U_3Si_2-related tetragonal crystal structure and orders antiferromagnetically below $T_N = 25$ K. The antiferromagnetic structure is characterized by a propagation vector $k = (00\frac{1}{2})$. The magnetism in U_2Rh_2Sn is found to be associated mainly with $5f$ states. However, both unpolarized and polarized neutron experiments reveal at low temperatures in zero field non-negligible magnetic moments also on Rh sites. U moments of 0.50(2) μ_B are directed along the tetragonal axis while Rh moments of 0.06(4) μ_B form a noncollinear arrangement confined to the basal plane. The response to applied magnetic field is highly anisotropic. Above ∼15 K the easy magnetization direction is along the tetragonal axis. At lower temperatures, however, a stronger response is found perpendicular to the c axis. While for the a axis no magnetic phase transition is observed up to 58 T, for the field applied at 1.8 K along the tetragonal axis we observe above 22.5 T a field-polarized state. A magnetic phase diagram for the field applied along the c axis is presented.

DOI: 10.1103/PhysRevB.95.174433

I. INTRODUCTION

Uranium based compounds are harboring a plethora of various physical properties and ground states that range from paramagnetism through spin fluctuations and heavy-fermionic states towards a long-range ferromagnetic or antiferromagnetic (AF) order [1]. In these materials superconductivity may coexist with a long-range magnetic order, and exotic states like hidden order in URu_2Si_2 can be realized as well [2–4]. All these materials show hybridization effects of the uranium $5f$ electron states with the wave functions of the s, p, and d wave functions of the surrounding ligands and conduction electrons. As the strength of hybridization depends not only on the geometry of the $5f$-containing atoms and distances to their neighbors but also on the type of ligands, studies on large groups of intermetallic compounds crystallizing in the same crystal structure play an important role in determining the general trends of the interplay between the direct $5f$–$5f$ overlap of electron wave functions, $5f$-ligand hybridization, and the resulting ground states [1]. Intermetallic compounds with a U_3Si_2-type structure constitute such a large group of compounds [5–10]. U_2Rh_2Sn adopts this structure which consists of two alternating planes, one containing only uranium atoms and the other Rh and Sn atoms. Projections along the a axis and the c axis are shown in Figs. 1(a) and 1(b), respectively.

In most uranium compounds U magnetic moments orient within a plane perpendicular to the shortest U-U links [9,10]. The generally accepted explanation is the increase of charge density in the U-U direction due to the direct $5f$–$5f$ wave-function overlap, which simultaneously increases the density of orbital currents and causes moments perpendicular to these directions [9]. However, some materials like U_2Rh_2Sn constitute an exception to this simple rule [10]. The shortest $5f$–$5f$ distance of $d_0 = 3.586$ Å is found along the c axis. Each U atom has two such nearest neighbors. The distances between U atoms within the basal plane are larger: There is one next-nearest neighbor at a distance $d_1 = 3.622$ Å and four second-next-nearest neighbors at a distance $d_2 = 3.902$ Å. Despite the fact that $d_0 < d_1$ the moments are reported to be directed along the shorter-distance direction [9,11]. In Fig. 1(c) we show the U atom sublattice with marked links and the equivalency of the U_2Rh_2Sn crystal structure with the Shastry-Sutherland lattice (SSL) [Fig. 1(d)] known to show magnetization plateaus [12]. Corresponding exchange interactions are denoted as J and J', respectively. In the SSL, magnetic moments orient perpendicular to the unique axis as the case of TbB_4 [13]. Although not shown in Fig. 1, Rh atoms form such a type of lattice as well.

U_2Rh_2Sn has been the subject of numerous studies that include crystal structure determination [5,6], dc and ac magnetic susceptibility [5,11,14,15], transport properties [16], high-field magnetization [7,8,17,18], specific heat [9,15], and neutron diffraction [9,11,19]. Except for a study by Pereira *et al.* [11] that reports low-field magnetic bulk properties and neutron diffraction of a U_2Rh_2Sn single crystal, all literature deals with polycrystalline samples. The magnetization process at high fields is reported to be quite unusual. Firstly, different measurements using different pulse lengths came to contradicting conclusions regarding the type of the magnetocrystalline anisotropy and secondly, the magnetization process is by itself highly unusual as it shows strong hysteretic behavior not only around the transition but also in the wide field range above it, i.e., in the polarized state.

The magnetic structure of U_2Rh_2Sn is reported to be AF, characterized by a propagation vector $k = (00\frac{1}{2})$ [9,11].

*prokes@helmholtz-berlin.de

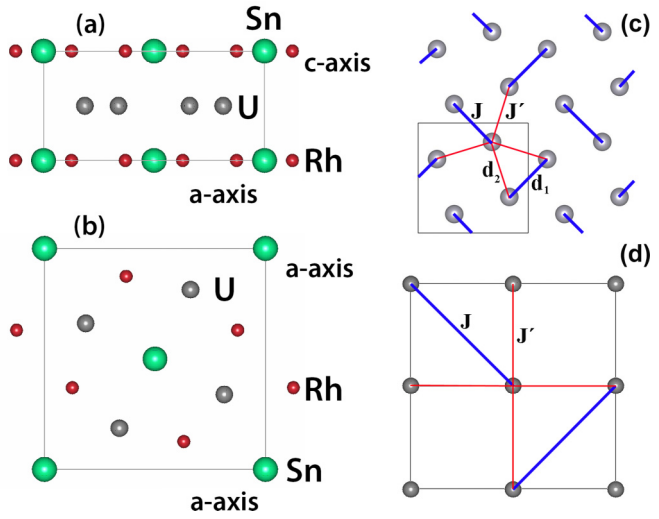

FIG. 1. Crystal structure of U_2Rh_2Sn as determined from neutron data projected along the a axis (a) and the c axis (b). Sn, U, and Rh atoms are shown by large, intermediate, and small spheres, respectively. A sublattice formed by U atoms projected along the tetragonal axis is shown in (c). The thick (blue) lines connect the next-nearest uranium neighbors (at a distance $d_1 = 3.622$ Å) and the thin line (red) the second-next-nearest neighbors (at a distance $d_2 = 3.902$ Å). Corresponding exchange interactions are denoted as J and J', respectively. The nearest U neighbors (at a distance $d_0 = 3.586$ Å) are found along the c axis. The rectangle represents one crystallographic unit cell projected along the c axis. U atoms form effectively a Shastry-Sutherland lattice as shown in (d). Rh atoms form this type of lattice as well.

Strongly reduced U moments of 0.38–0.53 μ_B are reported to be directed along the c axis. However, both the powder and single-crystalline neutron diffraction were inconclusive regarding the possible magnetic moment on Rh sites [9,11]. This point is important as it is not that uncommon that transition metal sites carry a substantial magnetic moment as a result of $5f$-ligand hybridization [20,21]. This fact together with a remaining controversy regarding the high-field magnetization process prompted us to re-investigate this system.

Keeping in mind that a large magnetocrystalline anisotropy is present in this system, we have prepared a single-crystalline sample and performed a series of bulk measurements in low and elevated magnetic fields applied along the principal axes. We report on magnetic bulk properties, electrical resistivity, specific heat, unpolarized and polarized neutron diffraction in fields up to 14.5 T and 6.2 T, respectively, and high-field magnetization in high magnetic fields up to 58 T leading to a construction of a magnetic phase diagram. Both polarized and unpolarized neutron diffraction experiments showed that non-negligible magnetic moments are associated with Rh sites oriented perpendicular to the c axis. This in turn may explain the unusual shape of the magnetization curve encountered above the metamagnetic transition that takes place at ∼22 T.

II. EXPERIMENTAL

A large single crystal of U_2Rh_2Sn has been grown using a modified tri-arc Czochralski technique in an ultrapure argon atmosphere from a stoichiometric melt of the constituent elements, which were melted several times before the growing process to obtain a homogeneous distribution of elements. The purity of used elements was Rh 99.95%, Sn99.995%, and U 99.5%. Uranium was additionally purified by the solid state electrotransport method [22].

The quality and homogeneity of the single crystal was determined using x-ray Laue diffraction and by scanning electron microscopy (SEM) equipped with a back scattered electron detector (BSE) and energy dispersive x-ray detector (EDX). The BSE contrast revealed the presence of two types of well localized impurities (approx. 3 vol. %) in an otherwise homogeneous single crystal. According to EDX analysis, the majority phase has a composition $U_{2.07(14)}Rh_{1.96(7)}Sn_{0.97(7)}$. The spurious impurities are unknown U-rich ternary phases with composition varying from $U_{3.3}Rh_2Sn$ to a phase containing 95% of uranium.

The single crystal was oriented by the Laue method and cut by a spark-erosion saw along the principal crystallographic axes. The top part of the ingot, pulverized under protective atmosphere, was used to obtain x-ray powder diffraction data using a Cu K-alpha Bruker powder diffractometer. The data were analyzed using a Rietveld type refinement with the Jana2006 software [23].

Electrical resistivity, magnetization $M(T)$, and the static magnetic susceptibility $\chi = M/H$, where H denotes the applied magnetic field, were measured between 2 and 300 K using the Quantum Design 14 T physical properties measurements system (PPMS), which is part of the Laboratory for Magnetic Measurements at the HZB (LaMMB). For the magnetization measurements the vibrating sample magnetometer (VSM) option was used. Resistivity measurements were performed using the standard four-point DC method. Temperature-dependent specific-heat measurements have been performed between 2 K and 35 K at constant magnetic fields up to 14 T applied along the c axis direction using PPMS. Typically, a 3% heat pulse was applied and the specific heat capacity determined using the relaxation method.

Pulsed high magnetic field measurements have been performed at the High Field Laboratory of the Helmholtz Zentrum Dresden-Rossendorf. We have used three small single crystals with weight between 30 and 44 mg. Crystals were oriented along the [100], [110], and [001] directions. The magnetization $M(H)$ measurements were performed between 1.8 K and 30 K in fields up to 58 T generated by discharging a capacitor bank producing 25 ms long magnetic field pulse. For the c axis direction we have collected data also at 640 mK achieved using a ^{3}He refrigerator. In this case, in order to minimize heating by eddy currents, we have utilized a longer pulse of 150 ms. The magnetic signal was detected in all cases by a compensated pick-up coil system and scaled to low-field magnetization and magnetic susceptibility data.

Neutron single-crystal diffraction experiments took place on the E4 and E5 instruments at the BER II reactor of the HZB. We have used a single crystal with dimensions $4 \times 4 \times 4$ mm^3. An incident wavelength $\lambda = 2.4$ Å selected with the PG (002) monochromator was utilized in both cases along with a set of $\lambda/2$ filters reducing the contamination of higher-order wavelength components to a level below 10^{-4}. The E4 diffractometer is equipped with a two-dimensional position sensitive ^{3}He-detector (200×200 mm^2) enabling an effective

mapping and detection of all the available diffracted signals. The superconducting split-pair coil cryomagnet capable of generating magnetic fields up to 14.5 T limited us to ±2.7 degrees from the scattering plane. The field has been applied along [001] and [110] directions.

In order to determine the crystal structure of U_2Rh_2Sn necessary for analysis of polarized neutron data, we have performed a measurement on a four-circle diffractometer E5 using a shorter neutron incident wavelength of 0.90 Å selected by a Cu monochromator. The E5 instrument is equipped with a two-dimensional position sensitive ^{3}He-detector (90×90 mm^2).

The crystal structure refinements were carried out with the program Xtal 3.4.4 [24] and the refinements of the magnetic structure have been performed using the program Fullprof (part of the Winplotr suite [25]). In the refinements, the nuclear scattering lengths $b(\mathrm{Sn}) = 6.23$ fm, $b(\mathrm{Rh}) = 5.88$ fm, and $b(\mathrm{U}) = 8.417$ fm were used [26].

A polarized neutron diffraction (PND) experiment has been carried out on a 5C1 diffractometer installed at the ORPHÉE 14 MW reactor of the Léon Brillouin Laboratory, CEA/CNRS Saclay. Here we have investigated a small (≈ 88 mg) single crystal originating from the same batch as crystals used for other studies. A polarizing Heusler $Cu_2MnAl(111)$ monochromator was used to select vertically polarized neutrons with wavelength $\lambda = 0.84$ Å from a hot source. An adiabatic cryoflipper is installed between the monochromator and a vertical superconducting magnet capable of producing 6.2 T. The polarization between different components is maintained using magnetic guides and the resulting incident beam polarization amounts to 88%.

The 5C1 diffractometer is equipped with a large ^{3}He position sensitive detector covering 120 degrees of the scattering angle, 5 degrees below and 18 degrees above the scattering plane. We have collected data at 30 K, i.e., at temperature that is a few K above the magnetic phase transition, in two orientations: with the sample's tetragonal axis parallel to the field direction and with the field applied perpendicular to it. The magnetic field of 6.2 T has been applied in the former geometry 2 degrees from the c axis, in the latter about 8 degrees from the a axis, within the plane perpendicular to the c axis. In both cases we have recorded 270 degrees of the samples's rotation and collected over 100 flipping ratios.

In the case of the treatment of magnetic intensities (both polarized and unpolarized), we assumed magnetic form factors of the U^{3+}/U^{4+} and Rh^{1+} type, respectively [27,28]. Using polarized neutron data, magnetic structure factors have been calculated using the Cambridge Crystallography Subroutine Library [29] suite programs. Spin densities were reconstructed using the software package PRIMA [30] that calculates the most probable distribution that is in agreement with the symmetry of the parent lattice, observed magnetic structure factors, and associated errors using the maximum entropy (MAXENT) method [31]. The resulting densities were drawn using the computer code VESTA [32].

III. RESULTS

A. Crystal structure

Refined parameters of the x-ray powder pattern are in good agreement with the literature [5,6,9,11]. However, additional low-intensity peaks not indexable within the main structure of U_2Rh_2Sn were detected as well. Since EDX measurements reveal a presence of a secondary phase with an enhanced uranium content as well, several common uranium compounds like various carbides and oxides were checked. However, all of them were rejected in the course of refinement as being the origin of these reflections.

Wide-angle diffraction single crystal data collected using the E4 diffractometer revealed that the quality of the crystal was acceptable although it has been found that a minority grain (≈ 6 vol.%) rotated by 1.6 degrees from the main grain exists. Moreover, reflections with $h = 2n + 1$ not compatible with the space group $P4/mbm$ were observed as well suggesting either a different space group or multiple scattering. The ratio between the 010 and 020 Bragg reflection of 0.15 excludes that these are due to $\lambda/2$ contamination. Although superstructure modifications are not uncommon in this group of compounds [33], a subsequent experiment on the E5 diffractometer proved that these reflections are due to multiple scattering.

In total 80 individual reflections (29 inequivalet ones) were measured using the E4 diffractometer at several B-T thermodynamic conditions and corrected for the Lorentz factor and extinction which was found to be negligible. The refinement of nuclear reflections collected above the proposed magnetic phase transition temperature in two different orientations lead to crystallographic parameters that are in good agreement with the x-ray data and literature [5,6]. The agreement factor was $R_F = 0.101$.

The appearance of $h00$ reflections with $h = 2n + 1$ prompted us to carry out so-called azimuthal ψ scans around the scattering vector of a reflection in question using the E5 diffractometer. It appeared that the intensities of these reflections diminish at particular positions of ψ, proving a presence of multiple scattering.

For the refinement of the crystal structure of U_2Rh_2Sn, we have collected on the E5 instrument a data set at 8 K using the incident wavelength $\lambda = 0.90$ Å 1182 reflections (303 inequivalent ones), all indexable within the space group $P4/mbm$, were used for the refinement. Lattice constants were determined from the orientational UB matrix calculated from 490 Bragg reflections. The fitted parameters are listed in Table I.

B. Magnetic bulk properties

In Fig. 2(a) the temperature dependences of the static magnetic susceptibility $\chi = M/H$ measured along the a and c axis in a field of 1 T are shown. Such an approach is valid only in the case where χ is field independent up to this field. As is shown below, the magnetization is (except for a limited temperature range around the magnetic phase transition) linear with the field (see Fig. 2). Indeed, values obtained for a field of 14 T are only slightly lower.

χ is highly anisotropic with the response along the c axis being much larger in the paramagnetic state. This qualifies this direction as the easy magnetization direction. The magnetic susceptibility measured along the [110] direction is identical to that measured along the a axis suggesting that the anisotropy within the basal plane is negligible. With lowering the

TABLE I. Crystal structure parameters of U_2Rh_2Sn as determined from the neutron data collected at 8 K on E5 using incident wavelength of $\lambda = 0.90$ Å. The thermal parameters U_{ij} (given in 100 Å^2) are in the form $\exp[-2\pi^2(U_{11}h^2a*^2 + 2U_{13}hla^*c^*)]$, where h, k, and l are indices of the relevant Bragg reflection and a^* and c^* are reciprocal lattice constants. For symmetry reasons the values U_{12} (for Sn only), U_{13}, and U_{23} of the atoms U, Rh, and Sn are equal to zero in this structure. For similar reasons, $U_{11} = U_{22}$ for all the atoms.

U_2Rh_2Sn		Space group:		$P4/mbm$		
Atomic positions:			Thermal parameters:			
Atom/Site	x	y	z	U_{11}	U_{33}	U_{12}
U/4h	0.1719(1)	$x + \frac{1}{2}$	$\frac{1}{2}$	0.39(5)	0.55(8)	0.06(4)
Rh/4g	0.3674(2)	$x + \frac{1}{2}$	0	0.39(7)	0.73(8)	−0.06(5)
Sn/2a	0	0	0	0.52(7)	0.5(1)	0
Cell parameters:						
a (Å)	7.449(1)					
c (Å)	3.5859(1)					
Agreement factor:			$R_F = 0.073$			

temperature the response along both a and c axis directions increases. Eventually, both temperature dependencies exhibit a distinct anomaly at 25 K marking the onset of magnetic ordering. Below this temperature new magnetic Bragg reflections appear at positions suggesting a doubling of the magnetic unit cell with respect to the crystallographic one. The magnetic ordering is therefore AF and the anomaly can be identified as the Néel temperature. These findings are in a good agreement with literature data [8,11,14]. At lower temperatures a significant drop of χ_c is observed. Notably, both curves cross around 15 K, leading to a reversed magnetic response at low temperatures. This finding is in a clear contradiction with previous results by Pereira *et al.* which reports that $\chi_a < \chi_c$ at all temperatures [11].

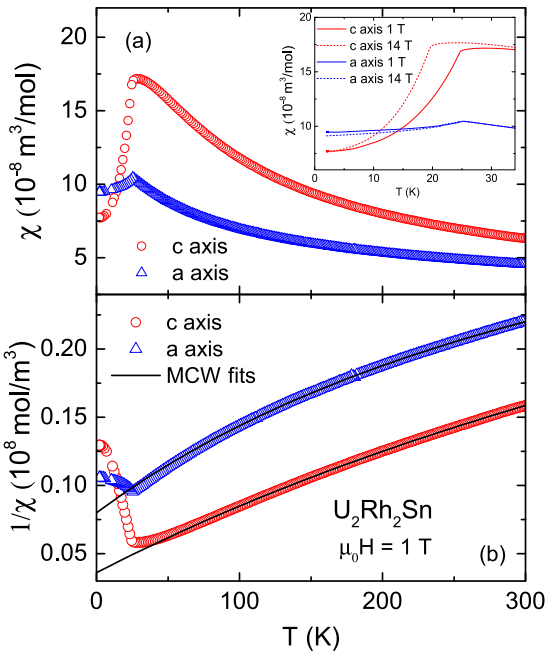

FIG. 2. Temperature dependence of the magnetic susceptibility $\chi(T)$ with a field of 1 T applied along the two principal directions (a). The inset magnifies the area around T_N showing also the data taken in 14 T. Panel (b) shows the temperature dependence of the inverse magnetic susceptibility (open points) together with the best fits to a modified Curie-Weiss law (full lines).

In the inset of Fig. 2(a) we show the temperature dependences of the magnetic susceptibilities measured at 1 T and 14 T. As can be seen, the anomaly shifts with magnetic field applied along the c axis significantly in contrast to the a axis direction where it stays pinned at 25 K. This corroborates a finding that the c axis direction is in the paramagnetic state the easy magnetization direction.

The magnetic susceptibility along both the a and the c directions follows at higher temperatures a modified Curie-Weiss (MCW) law according to the expression $\chi_c(T) = \chi_0 + C/(T - \theta_p)$, where χ_0 is the temperature independent term, C denotes the Curie constant, and θ_p is the paramagnetic Curie temperature. The best fit to this expression at temperatures between 70 and 300 K gives an excellent agreement with the experimental data [see the full lines through the points in Fig. 2(b)]. The refined temperature independent term χ_0 amounts to 2.3×10^{-8} m^3/mol and 1.8×10^{-8} m^3/mol for the a and the c axis direction, respectively (both per formula unit). The refined paramagnetic Curie temperatures θ_p amount to −84.5(0.2) K and −62.1(0.1) K for the a and c axis directions, respectively, documenting a predominantly AF exchange in U_2Rh_2Sn.

The refined effective moment obtained is 1.65(0.02) μ_B/U and 2.26(0.01) μ_B/U, for the a and the c axis direction, respectively. These values differ slightly from single crystal values reported by Pereira *et al.* [11] and powder measurements by Havela *et al.* [8]. We attribute the differences to possible influence of a small misalignment, impurities, fitting method, and/or temperature range in which the magnetic susceptibility was analyzed. Indeed, the best fit to a Curie-Weiss law performed above 250 K leads to an effective moment of 3.2 μ_B/U. This value is approaching the effective moment of a localized U^{3+} and U^{4+} (3.58 and 3.62 μ_B/U, respectively) moment.

Magnetization measurements for the a and c axes, M_a and M_c, as a function of applied static field up to 13 T are shown in Figs. 3(a) and 3(b), respectively. As can be seen, the magnetization measured along the a axis increases linearly with the applied field and is only very weakly dependent on

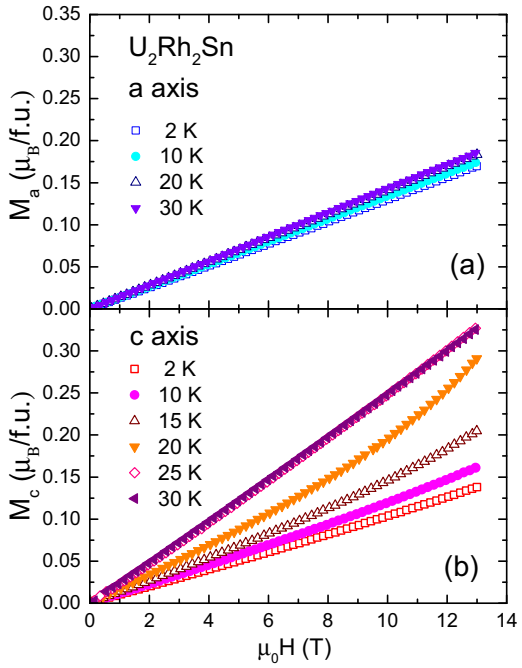

FIG. 3. Magnetization measurements as a function of magnetic field applied along the a axis (a) and along the c axis (b) at various temperatures measured using PPMS magnetometer.

the temperature. In contrast, the c axis magnetization that is linear with field at low temperatures shows in the vicinity of T_N at higher fields a significant upward curvature. This is very easily seen for the magnetization curve taken at 20 K. Above ∼30 K the response along the c axis is again linear. Although M_c is at 2 K and at all fields up to 13 T lower than the magnetization measured along the a axis it gains at temperatures above ≈ 15 K values that are larger than M_a. This finding corroborates the magnetic susceptibility results.

Magnetization measurements as a function of applied field up to 58 T taken at 2 K along the a and the c axes and along the [110] direction, are shown in Fig. 4. In agreement with the low field data, the magnetic response along the a axis ([100]) direction and the [110] direction remains very similar. Their dependences remain linear with field up to 58 T. In contrast, the magnetization measured along the tetragonal axis shows a distinct sharp metamagnetic transition (MT) located at 22.5 T on the increasing branch and at 22.1 T when the field is removed. The transition marks a modification of the low-field AF structure. The magnetization step across the MT amounts only to 0.1 μ_B/U and the magnetization curve shows at high fields only a very slow tendency towards saturation. The moment attained for the c axis at 58 T is 0.43 μ_B/U. These observations are in agreement with literature data taken on polycrystalline samples [17,18].

Above the MT the magnetization along the c axis increases monotonically but not in a trivial way. This observation, suggesting above MT a possible formation of a plateau similar to SSL materials [12], has prompted us to perform a measurement at 640 mK. A magnet with a six times longer pulse duration to minimize eddy current heating has been used. The measured magnetization curve exhibits, however, merely a single MT (see the inset of 4). We interpret this finding as

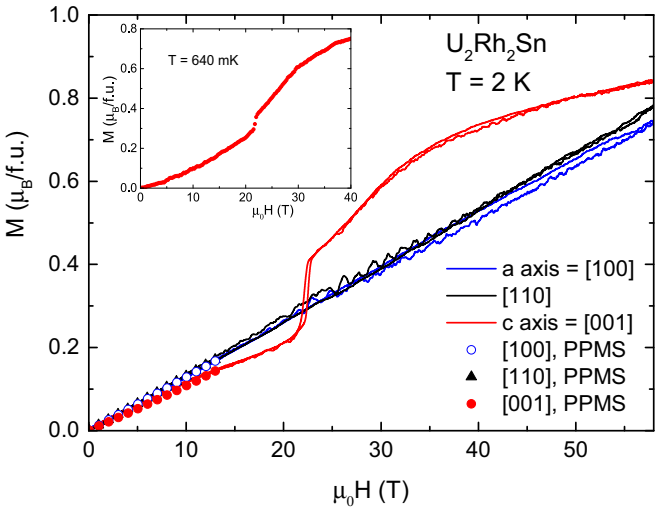

FIG. 4. High-field magnetization curves obtained at 2 K in pulse fields applied along [100], [110], and [001] directions together with the data (shown as full points) taken in static fields using PPMS. In the inset we show the magnetization curve obtained at 640 mK along the c axis using a magnet with a significantly longer pulse duration.

a consequence of a different duration of the two field sweeps and a different sensitivity of these measurements to dynamics of the magnetization process.

In Fig. 5 we show magnetization curves collected at various temperatures with increasing magnetic field applied along the c axis up to 58 T. The data have been normalized to measurements obtained using PPMS. As the temperature increases, the character of the magnetization process changes significantly. The magnetization step associated with the MT decreases and the transition itself broadens and shifts to lower fields. The transition can be still discerned in the data taken at 20 K. Simultaneously, the hysteresis of the transition (not shown) decreases with increasing temperature. Moreover, at low temperatures we observe a clear tendency towards saturation at high fields. This tendency is weaker

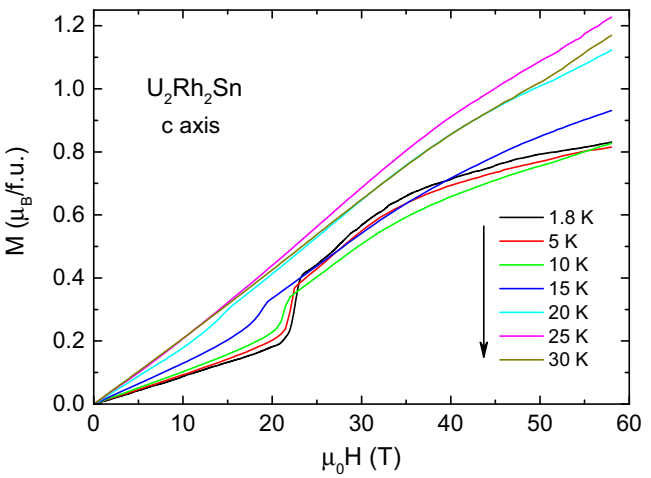

FIG. 5. High-field magnetization in increasing pulse fields applied along the c axis direction measured at different temperatures.

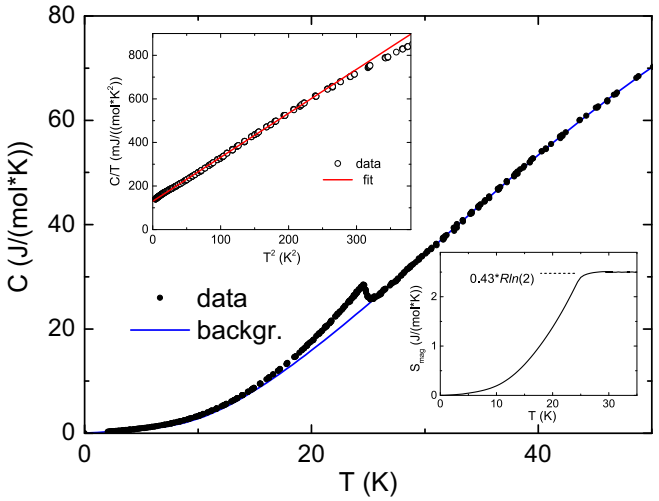

FIG. 6. The temperature dependence of the specific heat C of U_2Rh_2Sn single crystal measured in zero magnetic field. The solid line through measured data is the estimation of the phonon background as described in the main text. The lower inset shows the temperature development of the magnetic entropy S_{mag}. The top inset shows the low temperature part of the specific heat in the C/T vs T^2 representation together with the best fit to formula given in the main text.

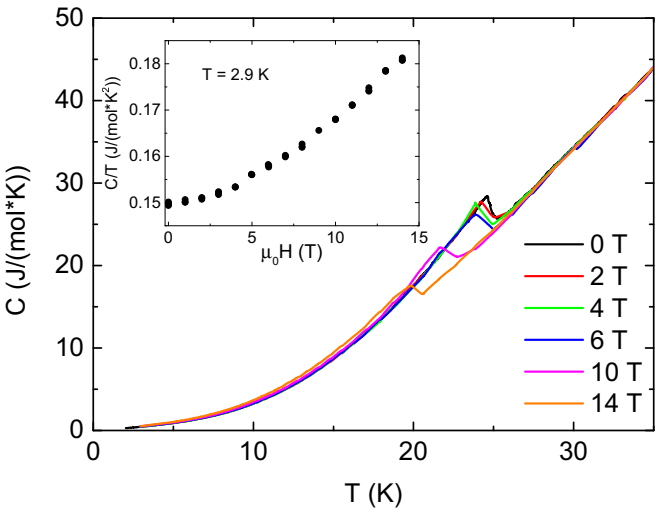

FIG. 7. The temperature dependence of the specific heat C of U_2Rh_2Sn single crystal measured in applied magnetic field up to 14 T directed along the tetragonal axis. In the inset we show the variation of the specific heat recorded at 2.9 K with field applied along the c axis.

above 15 K and lost at higher temperatures. The magnetization reached at the highest field stays at low temperatures almost constant but increases with increasing temperature and attains a maximum at T_N. At the moment it is not clear why the magnetization above T_N is larger than the saturated value at lower temperatures. One possibility is that dynamical effects including eddy currents make a reliable scaling to static low field values not possible. Another, more exotic model suggests that part of the U moment is quenched below the magnetic phase transition in analogy to URu_2Si_2 [3]. The response along the two remaining directions is very similar and linear with respect to the applied field up to 58 T at all temperatures without a sign of any phase transition.

C. Specific heat

In Fig. 6 we show the temperature dependence of the specific heat measured in zero external field. A relatively small but a clear anomaly in the temperature dependence of the specific heat around 25 K can be observed. The specific heat $C(T)$ can be fitted between 2 K and 14 K to a formula $C = \gamma T + \beta T^3$, where γ denotes the electronic low-temperature specific heat coefficient and β relates to the Debye temperature θ_D via expression $\theta_D^3 = 12\pi^4 R/5\beta$. The best fit to this formula yields $\gamma = 130.0(0.4)$ mJ /(molK^2) and $\theta_D = 168.1(0.7)$ K. These values are in agreement with literature data [9]. In the upper inset of Fig. 6 we present the experimental data together with the best fit in the C/T vs T^2 representation. In order to be able to estimate the magnetic entropy connected with the magnetic order a reliable estimate of the phonon and electronic contributions is needed. We have approximated the phonon contribution that dominates the specific heat data at temperatures above $T_N = 25$ K using the Debye specific heat model. The Debye temperature determined from the best fit in the temperature range 27–45 K amounts to $\theta_D' = 184.4(1.1)$ K, a value that agrees reasonably well with the $\theta_D = 168.1(0.7)$ K from the low-temperature fit. The sum of the electronic and phonon contributions is shown in the main panel of Fig. 6 by a solid line. The difference with respect to the experimental data can be interpreted as a magnetic specific heat C_{mag}. Magnetic entropy S_{mag} is obtained by integration of C_{mag}/T. In the lower inset of Fig. 6 the temperature dependence of the S_{mag}(T) documenting that above ≈ 25 K S_{mag} approaches a value of $0.43Rln(2)$, i.e., a value that is significantly smaller than a value expected for fully developed U magnetic moments, however, in agreement with literature [1,9]. Note that the S_{mag} is determined per two U atoms.

In Fig. 7 we show the temperature dependence of the U_2Rh_2Sn specific heat measured in zero external field and in fields up to 14 T applied along the tetragonal axis. The anomaly gets somewhat smeared out with increasing the applied field and shifts towards lower temperatures. The magnetic entropy obtained by integration of C_{mag}/T up to 30 K, i.e., in the same temperature range, does not change substantially as a function of applied field and remains nearly constant. This suggests that the magnetic entropy shifts merely to lower temperatures. Indeed, the isothermal specific heat increases at low temperatures slightly as a function of field. This is documented in the inset of Fig. 7, where we show the specific heat measured at 2.9 K divided by the temperature as a function of the applied field.

D. Electrical resistivity

In Fig. 8 we show the electrical resistivity ρ_c measured along the c axis in the temperature range between 2 and 300 K. The electrical resistivity is rather large at high temperatures (at 300 K, ρ_c, attains 127 $\mu\Omega$ cm) and increases slightly upon cooling. It exhibits a broad maximum around 200 K and

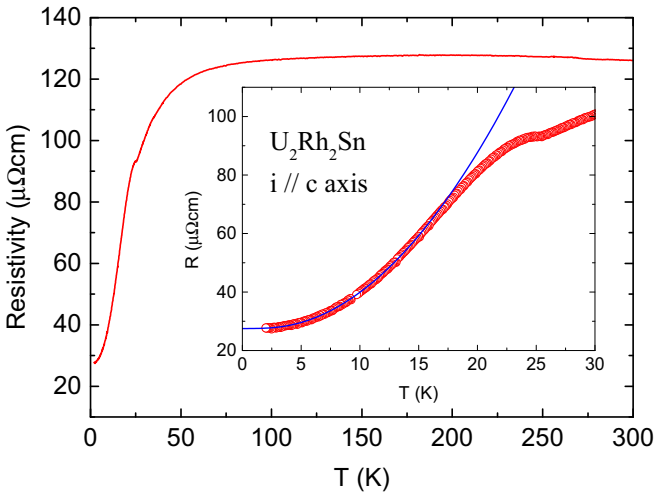

FIG. 8. Electrical resistivity of U_2Rh_2Sn single crystal measured along the c axis. The inset shows the low-temperature detail of the electrical resistivity curve to focus on the anomaly caused by the onset of antiferromagnetism and the best fit to the expression described in the main text.

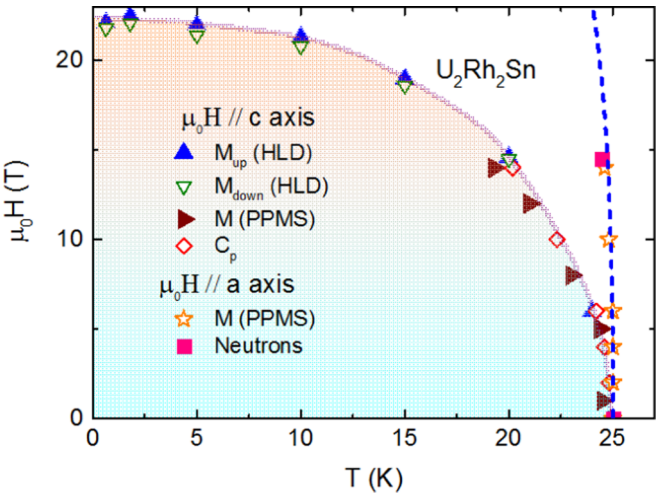

FIG. 9. Magnetic phase diagram of U_2Rh_2Sn for field applied along the c axis determined from high field pulse measurements (HLD) and magnetization and specific heat measurements using static fields. The magnetic phase boundary for field applied along the a axis is shown by the broken, nearly vertical line.

falls down strongly below 70 K. The electrical resistivity data show an anomaly at 25 K as shown in the inset of Fig. 8 that is connected with AF ordering and levels off in the low-temperature limit. These results are in good agreement with literature data [9,16].

The low-temperature part that is shown in the inset of Fig. 8 cannot be described by an ordinary Fermi-liquid dependence of the form $\rho(T) = \rho_0 + aT^n$ with $n = 2.0$. The best fit to data between 2 and 15 K yields $n = 2.29(1)$. However, even better agreement with data in the same temperature range is obtained for expression $\rho(T) = \rho_0 + aT^2 + bT(1 + 2T/\Delta)e^{-\Delta/T}$ yielding $\rho_0 = 27.5(2)\ \mu\Omega\,\mathrm{cm}$, $a = 0.025(8)\ \mu\Omega\,\mathrm{cm\,K^{-2}}$, $b = 0.59(2)\ \mu\Omega\,\mathrm{cm\,K^{-1}}$, and $\Delta = 7.7(1.7)$ K. The fit is shown in Fig. 8 by the solid line through the experimental points. This formula has been introduced in order to account for the influence of an energy gap Δ in the dispersion relation of magnetic excitations caused by strong electron-magnon coupling [34].

E. Magnetic phase diagram

Combining all the available experimental data allowed for construction of the magnetic phase diagram as shown in Fig. 9. All the measurements show that the magnetic field alters the magnetic order in U_2Rh_2Sn in a steplike manner only if it is applied along the tetragonal axis. This is documented by the invariance of the magnetic phase transition temperature $T_N = 25$ K and absence of any field-induced transition for field applied within the ab plane up to 58 T. For the a axis we observe that the $T_N = 25$ K is independent of field at least up to 14 T. For higher fields only measurements up to 58 T at constant temperatures are available leading to a conclusion that the low-field phase is not altered up to this field applied along the a axis. On the contrary, for the c axis we observe significant modifications.

Such a magnetic phase diagram is very similar to many other U-based compounds showing strong magnetocrystalline anisotropy [1]. In particular, it documents robustness of the magnetic order against the magnetic field applied perpendicular to the c axis. Such a behavior is conventionally explained by the direct $5f$–$5f$ electron wave functions overlap and their hybridization with ligand states that locks U moments along a specific direction [1,9].

F. Magnetic structure

As the temperature is lowered below the magnetic phase transition temperature $T_N = 25$ K, new Bragg reflections appear at positions indexable with a single propagation vector $k = (0,0,\frac{1}{2})$. This observation proves the existence of an AF order. In Fig. 10 we show a representative scan through the

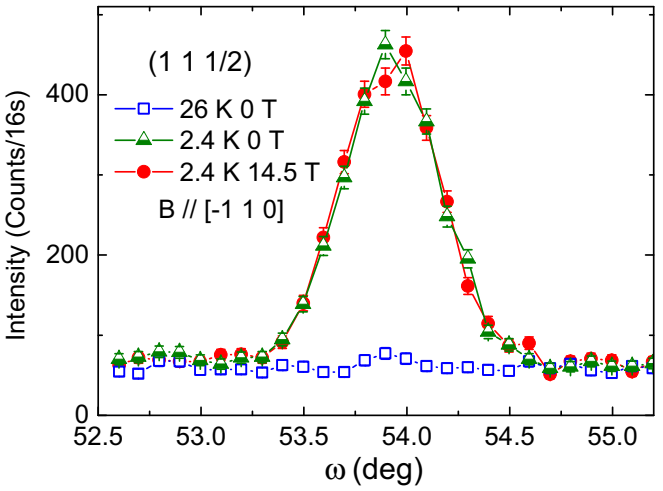

FIG. 10. Rocking curves through the $(1\ 1\ \frac{l}{2})$ magnetic Bragg reflection collected at 2.4 K and at 26 K (just above the magnetic phase transition) in zero field and at 2.4 K in a field of 14.5 T applied along the $[\bar{1}10]$ direction.

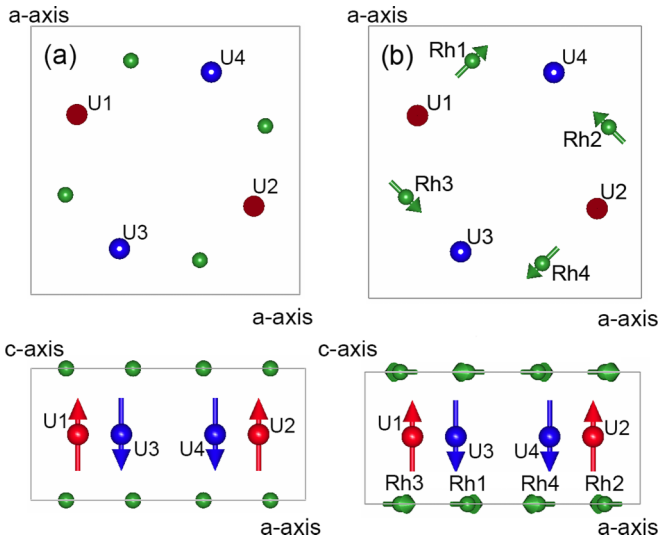

FIG. 11. Schematic representation of the AF structure of U_2Rh_2Sn as determined from the best fit of our neutron diffraction data taken at 2.4 K in zero external field to the model assuming the existence of only U moments (a). AF structure of U_2Rh_2Sn assuming the existence of both U and Rh moments is shown in (b). Rh moments were multiplied by a factor of five. Both structures are shown in two projections: along the tetragonal axis (top) and along the a axis (lower panel). Only half one magnetic unit cells are shown. Moment directions in the adjacent cells along the c axis are reversed.

$(1\ 1\ \frac{1}{2})$ magnetic Bragg reflection taken at 2 K and at 26 K in zero field and at 2.4 K in a field of 14.5 T applied along the $[\bar{1}10]$ direction. As it can be seen, the intensity of this reflection vanishes above T_N. No intensities are observed at any $(0\ 0\ \frac{l}{2})$ reciprocal space positions. These findings are entirely in agreement with the literature [9,11,35]. In total we have collected on the E4 diffractometer a set of 36 magnetic reflections (18 unique ones) at various positions within the magnetic phase diagram. For the refinement of the AF structure we have used a data set taken at 2.4 K in zero field. To obtain the magnetic moment values we have used the structural parameters as described in Table I and initially assumed that only U atoms carry magnetic moment.

In order to refine the magnetic structure one conventionally compares the intensity of magnetic reflections calculated from all possible magnetic structure models that are compatible with the observed magnetic propagation vector and the paramagnetic space group. These models are deduced by using a symmetry group analysis as developed by Bertaut [36]. Analysis for the propagation vector $k = (0,0,\frac{1}{2})$, site $4h$, and the space group $P4/mbm$ has been performed earlier and is available in the literature [19,35]. U moments are confined either within the basal plane or oriented in a collinear fashion along the c axis.

After testing all possibilities it became clear that only the model shown in Fig. 11(a) (in the original paper of Bourée *et al.* [35] as Γ_8) can explain the observed intensities satisfactorily. This model leads agreement to factors that are at least two or three times lower than for other models. The refined moment amounts to 0.55(1) μ_B/U and the agreement factor was $R_M = 0.051$. The moment value resulting from this fit is larger than the result obtained on powder sample [9] and in good agreement with the moment obtained by Pereira *et al.* [11]. Nevertheless, as magnetic moments on Rh sites cannot be excluded, we have performed the symmetry group analysis also for the $4g$ site taken by Rh atoms. The analysis leads for moments at the Rh $4g$ sites to very similar magnetic moment configurations as in the case of U moments at $4h$ sites. Rh moments are either confined to the basal plane or directed along the c axis. However, in many cases their directions are within one irreducible representation (irrep) perpendicular to U moments. In particular, in the case of the model associated with irrep Γ_8 described above are the Rh moments confined to the ab plane, in the case of Γ_3, reported for U_2Ni_2In are the U moments in plane but Ni moments along the c direction [9,19]. The best agreement is found for Γ_8 with U moments of 0.50(2) μ_B (along the c axis) and Rh moments of 0.06(4) μ_B (within the ab plane). The resulting AF structure is shown in Fig. 11(b). The agreement factor improved slightly to $R_M = 0.045$ with χ^2 dropping by few % as well. However, the refined Rh moments are very small and at the limit of the sensitivity of our unpolarized neutron diffraction experiment. The sensitivity to small moments can be improved in a polarized neutrons experiment that is described below.

In Figs. 2 and 10 we demonstrate also the robustness of the magnetic structure against the influence of the magnetic field applied at low temperature both along and perpendicular to the tetragonal axis. The intensities of nuclear reflections are not influenced up to the highest magnetic field of 14.5 T available with the superconducting magnet applied along the c axis. For this geometry we could not observe any magnetic reflections. If the magnetic structure would be alternated, there would be a small increase of intensities due to a ferromagnetic component visible on top of, e.g., 110 and 200 reflections. In the present experiment with field applied along the c axis we can conclude that the induced moment is less than $\approx 0.1\ \mu_B$/U at 14.5 T and 2 K.

In Fig. 12 we demonstrate that magnetic reflections are also not influenced at low temperatures if the field is applied along the $[\bar{1}10]$ direction. A sizable effect for this field orientation can be seen only in a very close vicinity of T_N. This is documented in Fig. 12 which shows the temperature dependence of the $(1\ 1\ \frac{1}{2})$ magnetic reflection measured with increasing temperature in zero field and in a field of 14.5 T. The intensity of this reflection continuously decreases with increasing temperature and vanishes around $T_N = 25$ K. There is a tiny shift negative in T_N and difference in the intensity of the reflection when a field is applied. An isothermal field scan taken at 23 K with decreasing field is shown in the form of color coded map in the inset of Fig. 12. It shows that the intensity of the $(1\ 1\ \frac{1}{2})$ magnetic reflection increases upon removal of the field. However, the increase is very tiny. Assuming that the magnetic structure remains stable up to T_N, the moment change between 14.5 T and zero field could be estimated to be less than 0.12 μ_B/U.

G. Polarized neutrons

The use of a polarized neutron beam is known to be very beneficial for observation of small field-induced magnetic moments. In the case of small ferromagnetic components that appear at the top of nuclear Bragg reflections is this

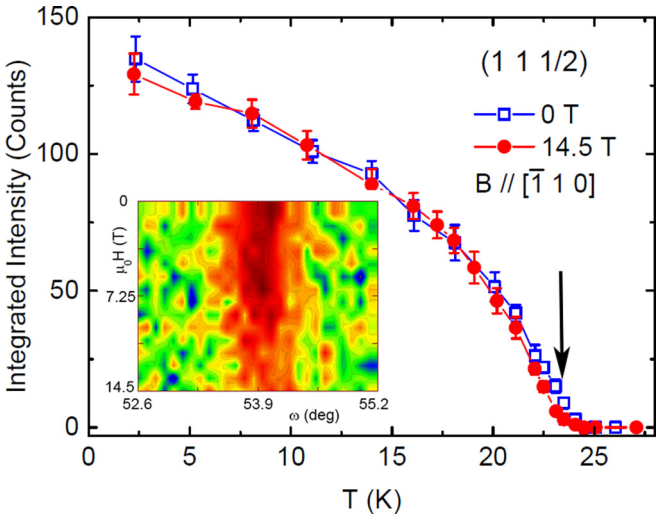

FIG. 12. Temperature dependence of the (1 1 $\frac{1}{2}$) magnetic Bragg reflection recorded with increasing temperature in zero field and in the field of 14.5 T applied along the [$\bar{1}$10] direction. The arrow in the main panel denotes conditions under which a field scan shown as a color coded map (shown in the inset) of intensities taken at the same reflection has been taken with decreasing field.

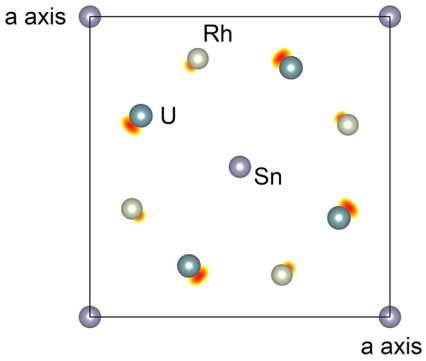

FIG. 13. Projection of the spin distribution in U_2Rh_2Sn onto a plane perpendicular to the c axis as obtained from the maximum entropy reconstruction from data collected at 30 K with a field of 6.2 T applied along the tetragonal axis. Only half of the unit cell along the c direction is projected. Densities around magnetic moments are restricted by an isosurface value of 0.01 $\mu_B/\text{Å}^3$. Densities below this level are not shown.

method (based on the interference between nuclear and magnetic contributions) especially indispensable [37]. In order to be able to extract the magnetic structure factors used in further refinement, one has to use reliable crystallographic information. In our case we have determined the crystal structure of U_2Rh_2Sn to a great precision at 8 K, at a not very different temperature at which polarized neutron experiment has been performed with a field of 6.2 T applied along principal axes. The magnetic structure factors have been obtained from a data set collected at 30 K using crystallographic data listed in Table I. Twenty six flipping ratios with a signal larger that one statistical deviation have been used in the analysis. However, it has to be noted that all the flipping ratios are close to unity and the fits to atomic models (with or without allowing Rh moments) are very unstable. It is therefore difficult to discriminate between different models. Another approach, a maximum entropy reconstruction [31], does not rely on any particular atomic model and yields the most probable spin density distribution compatible with experimental data and the underlying lattice symmetry.

In Fig. 13 we show such spin distributions reconstructed using this method. Two different significant magnetization clouds can be identified. One is situated in the vicinity of U atoms and the other, much smaller, in the vicinity of Rh atoms. The shift of the density maxima from atomic positions is in both cases small. Integration around these positions using relevant ionic radii [38] leads to magnetic moments of $\sim 0.02\,\mu_B$ at the U site and slightly less than $\sim 0.01\,\mu_B$ at Rh positions. The total magnetic moment associated with all the U and Rh sites in the unit cell amounts to $\sim 0.12\,\mu_B$, a value that should be compared with the magnetization value of $0.16\,\mu_B$ obtained from the magnetization measurements. The difference is attributed to a conduction-electron polarization.

A rather important result of this analysis is a small but non-negligible polarization associated with Rh sites. Such an observation that has been previously made in the case of other U-based compounds [1,20,21,39,40] is understood in terms of an anisotropic $5f$–d hybridization. However, the moment found on the transition metal atom is usually about one order of magnitude smaller than the leading magnetic moment associated with $5f$ states. For instance, a detailed study on a paramagnetic U_2Co_2Sn adopting the same crystal structure [41] shows U magnetic moments of 0.118 μ_B and Co moments of only 0.013 μ_B. In the case of U_2Rh_2Sn, however, we find that the Rh moment is only slightly less than a half of that at uranium. This seems to be not very compatible with the generally accepted picture regarding the hybridization-induced moment mechanism. On the other hand, it should be noted that our unpolarized neutron study indicated at low temperatures also a possible Rh moment. Furthermore, a similar study on isostructural U_2Ni_2In [9] suggested a significant moment residing at Ni sites attaining more than 60% of the uranium moment as well.

Unfortunately, the results of the measurement with the field perpendicular to the c axis are more uncertain. On one hand the spin distribution map shows well the clouds that can be associated with U and Rh sites. On the other it exhibits many noisy maxima that have no relation with any other atomic positions. We attribute this to the fact that the magnetic susceptibility along this direction is smaller than along the c axis and also the symmetry is reduced from the tetragonal one by the applied field. A much larger crystal is needed to perform a reliable experiment along this direction. The same holds also for measurement at low temperatures where the magnetic susceptibility along the c axis drops significantly.

IV. DISCUSSION AND CONCLUSIONS

In this study we have investigated in detail the magnetic, thermal, and electrical transport properties and determined the crystallographic and AF structure of the intermetallic compound U_2Rh_2Sn using a variety of experimental techniques. In agreement with literature, we have found that this system orders below $T_N = 25$ K. The AF phase transition

is manifested in temperature dependences of the magnetic susceptibility, the specific heat, electrical resistivity, and by an appearance of magnetic reflections indexable with $k = (0,0,\frac{1}{2})$. The magnetic entropy associated with the magnetic order is small and attains only a fraction of the value expected for a fully developed U moment. This suggests highly reduced U magnetic moment values. Indeed, U moments of 0.50–0.55 μ_B at 2.4 K were detected, Rh moments being even smaller. Such U value is greatly reduced with respect to U^{3+} or U^{4+} free ion values and suggests that the magnetism in U_2Rh_2Sn is governed by hybridization effects which induce Rh moments that are in the low-temperature limit about ten times smaller than at U sites. These results in turn agree with the best fits to a modified Curie-Weiss law. A strongly reduced effective magnetic moment and a signature of nonlocalized magnetic moments are obtained. A more localized $5f$ state is suggested by magnetic susceptibility data above 250 K.

The easy magnetization direction in the paramagnetic state is found to be along the tetragonal axis with a negligible anisotropy within the ab plane that is the hard magnetization direction. However, in contrast to previous studies we observe that the c axis is the easy magnetization axis only close and above the magnetic phase transition. At lower temperatures the response perpendicular to the c axis becomes stronger. Normally, a different behavior of perpendicular $\chi_\perp$ and longitudinal $\chi_\parallel$ magnetic susceptibility in a classical antiferromagnet can be explained by the fact that it is easier to tilt magnetic moments by the field than to increase their magnitudes, i.e., one expects $\chi_\perp > \chi_\parallel$ below T_N. This is not the case of uniaxial U-based systems where the anisotropy energy is so strong that any tilt from the unique axis is impossible leading to $\chi_\perp < \chi_\parallel$ at all temperatures [1]. In the present system the $\chi_\parallel = \chi_c$ is larger than $\chi_\perp$ only in the vicinity and above the T_N but smaller in the low temperature region.

Neutron diffraction experiments proved that the magnetism in U_2Rh_2Sn is associated mainly with $5f$ states. However, a significant contribution originating from Rh electronic states is found as well. The observed magnetic structure might account for the peculiar temperature dependence of the magnetic susceptibility. Comparing the zero field unpolarized neutron results at 2.4 K with polarized data obtained above the T_N we conclude that U and Rh sites might contribute to the magnetic susceptibility at different temperatures differently. At low temperatures are U moments of 0.50(2) μ_B oriented along the c axis and can contribute to χ_c only via changing their magnitude. Strong anisotropy does not allow them to be tilted from the c axis direction significantly. Still, $\chi_\perp > \chi_\parallel$ is observed. The Rh moments that are about ten times smaller are confined in a nonlinear fashion to the basal plane due to a necessity to belong to the same irrep. They can thus contribute both to the χ_c and χ_{ab} by their tilting away from the [110] type planes. We therefore attribute the peculiar behavior of $\chi(T)$ at low temperatures to the existence of Rh moments.

The above mentioned explanation of the susceptibility behavior relies on the assumption that the U moment sublattice in U_2Rh_2Sn exhibits inherently a uniaxial type of anisotropy that does not change with temperature. However, a generally accepted hybridization-induced anisotropy considers all contributions to an anisotropic hybridization and the direct $5f$–$5f$ wave function overlap. As the hybridization increases with shortening the interatomic distances, it is expected that the contribution from the latter mechanism would lead to U moments that lie within the basal plane. The $5f$–d hybridization would support this configuration as well because the Rh atoms lie outside the U-basal plane [see Fig. 1(a)]. Apparently, the experiment shows that U moments orient along the c axis. It should be, however, mentioned that for each U atom there is one next-nearest (NN) U neighbor and further four second-next-nearest (SNN) U neighbors at distances that are only 1.00% and 8.81% larger than the nearest neighbors found along the c axis. A competition between in-plane and out-of plane hybridization can be thus expected.

As mentioned above, both Rh and U sublattices in U_2Rh_2Sn map onto an effective 3D Shastry-Sutherland lattice. It is interesting to note that, considering only U moments, the observed AF structure belongs to one of the possible magnetic structures in zero magnetic field realized in an Ising system—the so-called Néel state [12]. The NN U moments at a distance of d_1 [exchange J in Fig. 1(c)] are coupled ferromagnetically (thus, $J > 0$) and do not form within the ab plane AF dimers. On the contrary, all couplings between SNN U neighbors are AF ($J' < 0$). Such a coupling would indicate $|J| < |J'|$. For comparison, in TmB_4 and TbB_4, where $4f$ moments lie within the basal plane, the $J < 0$ and $|J| > |J'|$ [13,42]. A further difference is that the coupling along the c axis is in U_2Rh_2Sn AF and in TmB_4 ferromagnetic. The situation within the Rh magnetic sublattice is more complex as the moments are noncollinear.

The high-field magnetization experiments in pulsed fields up to 58 T with field applied along the $c = [001]$ direction reveal that the MT shifts with increasing temperature towards lower fields. The response along the two remaining directions is very similar and linear with respect to the applied field up to 58 T at all temperatures without a signature of a phase transition. A magnetic phase diagram has been constructed. The magnetization attained at low temperatures at the highest field applied along the c axis of 0.43 μ_B/U is to be compared with the neutron value found for the zero-field AF state. The discrepancy along with a rather large high-field magnetic susceptibility without a clear saturation at even 58 T suggests that U moments are stabilized by the magnetic field. A complex magnetization curve for the field applied along the tetragonal axis suggests that the magnetization process is not of a simple spin-flip type. It is to be expected that a contribution from Rh moments that make at low temperatures a complicated noncollinear arrangement similar to SSL system, plays an important role. However, a search for possible magnetic states with fractionalized magnetization values (as observed in TmB_4 [42] or $SrCu_2(BO_3)_2$ [43]) was not successful. Nevertheless, in the view of the high critical field applied along the tetragonal axis necessary to destroy the ground-state AF structure of 22.5 T and create presumably only partially ferromagnetically aligned U and Rh moments it would be interesting to perform a high-field neutron diffraction experiment using the 26 T HFM-EXED facility [44].

ACKNOWLEDGMENTS

We acknowledge the support of the HLD at HZDR, member of the European Magnetic Field Laboratory (EMFL). We

acknowledge also allocated beam time at the laboratoire Léon Brillouin Saclay and technical support received. Experiments were performed partially in MLTL (http://mltl.eu/) funded by Ministry of Education, Youth and Sports of the Czech Republic within the program of Czech Research Infrastructures (Project No. LM2011025). This work was supported in part by the project 16-03593S of the Czech Science Foundation. We also acknowledge Helmholtz Association for financial support. We would like to thank R. Wimpory from HZB for checking our paper.

[1] V. Sechovský and L. Havela, *Handbook of Magnetic Materials*, edited by K. H. J. Buschow (North Holland, Amsterdam, 1998), Vol. 11, pp. 1–289.
[2] T. T. M. Palstra, A. A. Menovsky, J. van den Berg, A. J. Dirkmaat, P. H. Kes, G. J. Nieuwenhuys, and J. A. Mydosh, Phys. Rev. Lett. **55**, 2727 (1985).
[3] J. A. Mydosh and P. M. Oppeneer, Rev. Mod. Phys. **83**, 1301 (2011).
[4] D. Aoki, A. Huxley, E. Ressouche, D. Braithwaite, J. Flouquet, J. P. Brison, E. Lhotel, and C. Paulsen, Nature (London) **413**, 613 (2001).
[5] M. N. Peron, Y. Kergadallan, J. Rebizant, D. Meyer, S. Zwirner, L. Havela, H. Nakotte, J. C. Spirlet, G. M. Kalvius, E. Colineau, J. L. Oddou, C. Jeandey, J. P. Sanchez, and J. M. Winand, J. Alloys Compd. **201**, 203 (1993).
[6] F. Mirambet, P. Gravereau, B. Chevalier, L. Trut, and J. Etourneau, J. Alloys Compd. **191**, L1 (1993).
[7] H. Nakotte, K. Prokeš, E. Brück, N. Tang, F. R. de Boer, P. Svoboda, V. Sechovský, L. Havela, J. M. Winand, A. Seret, J. Rebizant, and J. C. Spirlet, Physica B (Amsterdam) **201**, 247 (1994).
[8] L. Havela, V. Sechovský, P. Svoboda, H. Nakotte, K. Prokeš, F. R. de Boer, A. Seret, J. M. Winand, J. Rebizant, J. Spirlet, A. Purwanto, and R. A. Robinson, J. Magn. Magn. Mater. **140-144**, 1367 (1995).
[9] H. Nakotte, A. Purwanto, R. A. Robinson, K. Prokeš, J. C. P. Klaasse, P. F. de Châtel, F. R. de Boer, L. Havela, V. Sechovský, L. C. J. Pereira, A. Seret, J. Rebizant, J. C. Spirlet, and F. Trouw, Phys. Rev. B **53**, 3263 (1996).
[10] V. Sechovský, L. Havela, H. Nakotte, F. R. de Boer, and E. Brück, J. Alloys Compd. **207–208**, 221 (1994).
[11] L. C. J. Pereira, J. A. Paixão, P. Estrela, M. Godinho, F. Boudarot, M. Bonnet, J. Rebizant, J. C. Spirlet, and M. Almeida, J. Phys. Condens. Matter **8**, 11167 (1996).
[12] B. S. Shastry and B. Sutherland, Physica B (Amsterdam) **108**, 1069 (1981).
[13] T. Matsumura, D. Okuyama, and Y. Murakami, J. Phys. Soc. Jpn. **76**, 015001 (2007).
[14] V. H. Tran, Z. Zolnierek, A. J. Zaleski, and H. Noél, Solid State Commun. **101**, 709 (1997).
[15] L. Havela, V. Sechovský, P. Svoboda, M. Diviš, H. Nakotte, K. Prokeš, F. R. de Boer, A. Purwanto, R. A. Robinson, A. Seret, J. M. Winand, J. Rebizant, J. C. Spirlet, M. Richter, and H. Eschrig, J. Appl. Phys. **76**, 6214 (1994).
[16] A. M. Strydom, P. de V. du Plessis, and V. V. Gridin, Physica B (Amsterdam) **225**, 89 (1996).
[17] F. R. de Boer, K. Kindo, H. Nakotte, K. Prokeš, and V. Sechovský, Physica B (Amsterdam) **246**, 129 (1998).
[18] T. Fukushima, S. Matsuyama, T. Kumada, K. Kindo, K. Prokeš, H. Nakotte, F. R. de Boer, L. Havela, V. Sechovský, J. M. Winand, J. Rebizant, and J. C. Spirlet, Physica B (Amsterdam) **211**, 142 (1995).
[19] F. Bourée, B. Chevalier, L. Fournés, F. Mirambet, T. Roisnel, V. H. Tran, and Z. Zolnierek, J. Magn. Magn. Mater. **138**, 307 (1994).
[20] J. A. Paixão, G. H. Lander, P. J. Brown, H. Nakotte, F. R. de Boer, and E. Brück, J. Phys. Condens. Matter **4**, 829 (1992).
[21] P. Javorský, V. Sechovský, J. Schweizer, F. Bourdarot, E. Lelièvre-Berna, A. V. Andreev, and Y. Shiokawa, Phys. Rev. B **63**, 064423 (2001).
[22] Y. Haga, T. Honma, E. Yamamoto, H. Ohkuni, Y. Onuki, M. Ito, and N. Kimura, Jpn. J. Appl. Phys. **37**, 3604 (1998).
[23] V. Petříček, M. Dušek, and L. Palatinus, Z. Kristallogr. **229**, 345 (2014).
[24] S. R. Hall, G. S. D. King, and J. M. Stewart, Eds., Xtal3.4 Users Manual. University of Australia: Lamb, Perth (1995).
[25] T. Roisnel and J. Rodríguez-Carvajal, Mater. Sci. Forum **378–381**, 118 (2001).
[26] V. F. Sears, in *International Tables for Crystallography*, edited by A. J. C. Wilson (Kluwer Academic Publisher, Dordrecht/Boston/London, 1995), Vol. C., p. 383.
[27] A. J. Freeman, J. P. Desclaux, G. H. Lander, and J. Faber Jr., Phys. Rev. B **13**, 1168 (1976).
[28] G. H. Lander, M. S. S. Brooks, and B. Johansson, Phys. Rev. B **43**, 13672 (1991).
[29] P. J. Brown and J. C. Matthewman, The Cambridge Crystallography Subroutine Library, Mark 4 Users Manual, Rutherford Appleton Laboratory Report (1993).
[30] F. Izumi and R. A. Dilanian, *Recent Research Developments in Physics, Part II* (3Transworld Research Network, Trivandrum 2002), p. 699.
[31] J. Skilling and S. F. Gull, in *Maximum Entropy and Bayesian Methods in Inverse Problems*, edited by C. Ray Smith and W. T. Grandy Jr., (D. Reidel Publishing Comp., Dordrecht, 1985), p. 83.
[32] K. Momma and F. Izumi, J. Appl. Crystallogr. **44**, 1272 (2011).
[33] K. Prokeš, P. Svoboda, A. Kolomiets, V. Sechovský, H. Nakotte, F. R. de Boer, J. M. Winand, J. Rebizant, and J. C. Spirlet, J. Magn. Magn. Mater. **202**, 451 (1999).
[34] N. H. Andersen and H. Smith, Phys. Rev. B **19**, 384 (1979).
[35] J. Rodríguez-Carvajal and F. Bourée, EPJ Web Conf. **22**, 00010 (2012).
[36] E. F. Bertaut, J. Magn. Magn. Mater. **24**, 267 (1981).
[37] B. M. T. Willis, *Thermal Neutron Diffraction* (Oxford University Press, Oxford, 1970), p. 190.
[38] R. D. Shannon, Acta Crystallogr. Sect. A **32**, 751 (1976).
[39] K. Prokeš and A. Gukasov, Phys. Rev. B **79**, 024406 (2009).
[40] K. Prokeš, A. de Visser, Y. K. Huang, B. Fak, and E. Ressouche, Phys. Rev. B **81**, 180407(R) (2010).

[41] J. A. Paixão, L. C. J. Pereira, P. Estrela, M. Godinho, M. Almeida, L. Paolasini, M. Bonnet, J. Rebizant, and J. C. Spirlet, J. Phys. Condens. Matter **11**, 2115 (1999).

[42] K. Siemensmeyer, E. Wulf, H.-J. Mikeska, K. Flachbart, S. Gabani, S. Matáš, P. Priputen, A. Efdokimova, and N. Shitsevalova, Phys. Rev. Lett. **101**, 177201 (2008).

[43] Y. H. Matsuda, N. Abe, S. Takeyama, H. Kageyama, P. Corboz, A. Honecker, S. R. Manmana, G. R. Foltin, K. P. Schmidt, and F. Mila, Phys. Rev. Lett. **111**, 137204 (2013).

[44] P. Smeibidl, A. Tennant, H. Ehmler, and M. Bird, J. Low. Temp. Phys. **159**, 402 (2010).